Effects of temperature and pressure on the crystal structure of forsterite

Robert M. Hazen[1]

Harvard University, Department of Geological Sciences
Cambridge, Massachusetts 02138

Abstract

The crystal structure of synthetic forsterite has been studied as a function of temperature and pressure. Crystal structures have been refined from three-dimensional diffraction data collected at temperatures from −196°C to 1020°C and at pressures to 50 kbar. Volume compressibility and thermal expansion of individual magnesium octahedra are comparable to those of bulk foresterite. However, the silicon tetrahedron neither expands nor compresses within the range of conditions investigated. Thus, changes in Mg–O bond distances account for virtually all of forsterite's volume response to changes in temperature and pressure. Short Mg–O bonds vary significantly less with temperature and pressure than do long bonds, implying that shorter bonds are stronger. Octahedral distortions increase with temperature, but show no strong trends with increasing pressure.

Introduction

The characterization of minerals at high pressures and temperatures is an essential part of the earth sciences. Many physical properties of minerals including compressibility, thermal expansivity, and electrical conductivity are functions of temperature and pressure. Since a solid's physical properties are a direct consequence of its atomic arrangement, the continuous variation of atomic positions resulting from changes in T and P may thus be used to understand more fully the variation of physical properties with these intensive parameters. The principal objective of this study is to determine the atomic coordinates and thermal vibration parameters of magnesian olivine at a variety of temperatures and pressures in order better to define the equation of state of this important mineral.

The crystal structure of olivine was first determined by Bragg and Brown (1926); subsequent refinements were reported by Belov *et al.* (1951), Hanke and Zemann (1963), Birle *et al.* (1968), and Brown (1970). Lattice parameters of magnesian olivine have been evaluated by many authors (*e.g.* Louisnathan and Smith, 1968). Thermal expansion of olivine has been studied by several investigators including Kozu *et al.* (1934), Rigby *et al.* (1946), Skinner (1962), and Soga

and Anderson (1967). More recently, variations of crystal structure with temperature have been reported for pure forsterite and $Fo_{38}Fa_{62}$ (Smyth and Hazen, 1973), $Fo_{69}Fa_{31}$ (Brown and Prewitt, 1973), and pure fayalite (Smyth, 1975). Compressibility studies on olivine are numerous, and data of Bridgman (1948), Olinger and Duba (1971), and Schock *et al.* (1972) are frequently cited. Recent studies of Olinger and Halleck (1975) offer improved values for linear and volume compressibilities of olivine.

Olivine has two crystallographically distinct octahedral sites, one tetrahedral site, and three distinct oxygen positions. It displays significant deviations from ideal close-packing of oxygens, and these deviations are most conveniently visualized in terms of distortions of the octahedral and tetrahedral cation coordination polyhedra from their regular forms (compare Fig. 1a and Fig. 1b). The $M(1)$ site has $\bar{1}$ symmetry, and its coordination polyhedron approximates an octahedron flattened along a three-fold axis. The $M(2)$ octahedron, which has mirror symmetry, has larger average M–O distances than $M(1)$, and does not approximate any simple distortion model (Dollase, 1974). As noted by Brown (1970), the three olivine cation polyhedra have a number of oxygen–oxygen edges in common, including two between adjacent $M(1)$'s, two between $M(1)$ and $M(2)$, two between $M(1)$ and Si, and one between $M(2)$ and Si. Distortions of the hexagonal
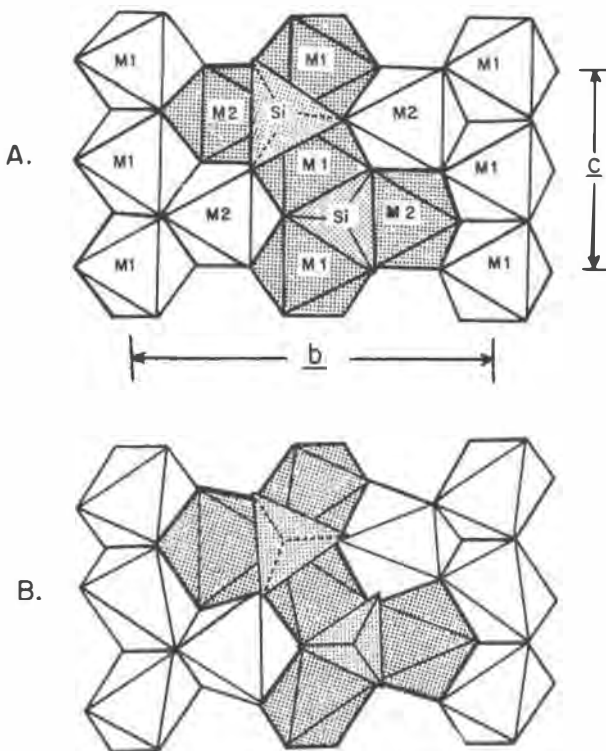
FIG. 1. Olivine crystal structure: A—ideal HCP model, B—actual structure, (after Brown, 1970).

close-packed oxygen array have been related to cation–cation repulsions across these shared edges in agreement with Pauling's third rule.

Experimental

Specimen description

Colorless and transparent single crystals of synthetic forsterite have been manufactured by the Crystal Products Division of Union Carbide Corporation, and were kindly provided by Professor T. J. Shankland. This essentially pure forsterite has a reported composition of 99.99 + percent Mg_2SiO_4, and the indices of refraction are $\alpha = 1.635 \pm 0.002$, $\beta = 1.650 \pm 0.002$, and $\gamma = 1.670 \pm 0.002$, which correspond to reported values for pure magnesian olivine (Heinriques, 1957). The crystals are optically free of fractures or other visible defects, and a good (010) cleavage is present. An irregular crystal of approximately $400 \times 300 \times 300$ μm maximum dimensions was selected for preliminary X-ray study. A suite of a-, b-, and c-axis precession photographs was obtained to confirm previous unit-cell and symmetry determinations. A diffraction symbol of $mmmPbn$- was observed, which corresponds to the reported olivine space group $Pbnm$.

Unit-cell dimensions of forsterite were determined on the oriented single crystal from precision back-reflection Weissenberg photographs. Refinement of 82 diffraction spot pairs yielded orthorhombic cell parameters of $a = 4.7535 \pm 0.0004$, $b = 10.1943 \pm 0.0005$, and $c = 5.9807 \pm 0.0004$ Å, with a resulting unit-cell volume of 289.80 ± 0.05 Å^3. These values closely agree with determinations by Yoder and Sahama (1957).

Data collection and instrumentation

Procedures for data collection from single crystals at room temperature, liquid-nitrogen temperature, and high temperature are described by Hazen (1976), while high-pressure X-ray diffraction techniques were similar to those of Hazen and Burnham (1974, 1975). High-pressure diffraction data have been corrected for diamond pressure cell absorption as well as specimen absorption (Hazen, 1976).

Results

Room temperature

A reference room-temperature and pressure structure refinement was made with 956 observed diffrac-

TABLE 1A. Forsterite unit-cell parameters from 23° to 1105°C

$T(^{\circ}C)$	$a(Å)$	$b(Å)$	$c(Å)$	$vol(Å^3)$
23	4.752(3)*	10.193(8)	5.977(5)	289.5(3)
180	4.758(5)	10.212(10)	5.991(6)	291.1(5)
305	4.765(5)	10.231(10)	5.998(6)	292.4(5)
450	4.767(3)	10.248(8)	6.009(5)	293.6(3)
610	4.775(5)	10.273(10)	6.023(6)	295.5(5)
750	4.780(3)	10.292(8)	6.032(5)	296.8(3)
900	4.785(7)	10.33(1)	6.047(9)	298.9(8)
1020	4.797(7)	10.35(2)	6.058(8)	300.7(12)
1105	4.805(7)		6.069(8)	

* Parenthesized figures refer to the esd of least units cited.

tion maxima representing all *hkl*'s in one octant of reciprocal space from 5° to 80° 2θ (MoKα). Of 1096 measured reflections, 116 including all 90 space-group extinct reflections, were unobserved. In addition, 24 of the strongest reflections, for which $|F_{obs}| \ll |F_{calc}|$, were rejected due to presumed secondary extinction. A calculated linear absorption coefficient of 10.594 cm^{-1} was applied, and transmission factors varied from 78 to 83 percent. Refinement of forsterite included 40 variables, representing 11 atomic positional parameters, 28 anisotropic vibrational parameters, and a scale factor. A weighted *R*-factor of 4.8 percent (4.9 percent unweighted) was obtained for this refinement. Forsterite refinement conditions, positional parameters, and temperature factors are listed in Tables 1, 2, and 3. Room temperature and pressure values are in close agreement with previous 23°C forsterite refinements by Birle *et al.* (1968) and Brown (1970).

Cell dimension and structural factor measurement at −196° to 1105°C

Forsterite unit-cell parameters and structure factors were measured at several temperatures from −196°C to above 1000°C. Preliminary results of the high-temperature portion of this study were reported by Smyth and Hazen (1973). The crystal chosen for high-temperature work by Smyth and Hazen was mounted in air directly on the join of the Pt/Pt$_{90}$Rh$_{10}$

thermocouple by natural adhesion to hot platinum. Unit-cell constants and intensity data were collected first at 23°C and then at *reported* temperatures of 300°, 600°, and 900° (see below).

In the present study, the crystal was mounted within a silica capillary, and unit-cell constants of forsterite were measured at temperatures to 1105°C (see Table 1a). An attempt at a 1020°C data collection was then made, but fewer than 150 diffractions were measured before the heater burned out. During the rapid cooling following heater failure, the silica capillary fractured and the crystal was lost. Thus, it was not possible to recheck the crystal at room temperature.

Another forsterite crystal of approximately rectangular shape, 200 × 180 × 120 μm, was mounted on a copper pin; unit-cell and intensity data were collected at liquid-nitrogen temperature using the Cryo-Tip system. Unit-cell parameters were redetermined following the low-temperature study, and were unchanged from previous room-temperature measurements. In each of the six structure refinements, made at −196°, 23°, 300°, 600°, 900°, and 1020°C, all *Pbnm* space group–extinct reflections were unobserved. From 6 to 24 of the strongest reflections were rejected from each refinement due to presumed secondary extinction (*i.e.*, $|F_{obs}| \ll |F_{calc}|$). Results are presented in Tables 1, 2, and 3, in the same format as that of Brown (1970) for ease of comparison.

TABLE 1B.   Forsterite unit-cell parameters and refinement conditions

T (°C)	P	Conditions	a (Å)	b (Å)	c (Å)	vol (Å^3)	wR(%)[a]	R(%)[a]	No. of Measurements	No. of Observed	No. of Rejected[a]
23	1 atm	Standard mount	4.7535(4)[b]	10.1943(5)	5.9807(4)	289.80(5)	4.8	4.9	1096	956	24
~350	"	Thermocouple[c] mount	4.763(5)	10.24(1)	5.999(6)	292.6(5)	5.4	5.6	663	569	7
~675	"	"[c]	4.778(5)	10.29(1)	6.017(6)	296.0(5)	5.7	5.9	676	564	6
~1000	"	"[c]	4.795(5)	10.36(1)	6.060(6)	300.8(5)	5.5	5.9	686	565	8
1020	"	Silica capillary mount	4.798(5)	10.36(1)	6.068(6)	301.4(5)	11.1[d]	12.9[d]	135	108	9
−196	"	Cryo-Tip mount	4.746(5)	10.18(1)	5.976(6)	288.6(5)	4.9	5.5	742	686	13
23	20kb	Pressure cell	4.743(5)	10.09(1)	5.954(6)	285.0(5)	7.0[d]	9.4[d]	969	329	3
23	40kb	"	4.734(5)	10.02(1)	5.940(6)	281.8(5)	7.3[d]	9.6[d]	964	374	6
23	50kb	"	4.712(5)	9.97(1)	5.955(6)	279.7(5)	9.8[d]	12.3[d]	962	332	13
23	1 atm	Standard mount (after high P)	4.749(5)	10.19(1)	5.980(6)	289.5(5)	3.9	4.2	1026	790	2

a) $||F_{obs}| - |F_{calc}|| \geq 3.0$

b) Parenthesized figures refer to the esd of least units cited.

c) Data of Smyth and Hazen (1973), with corrected temperature estimates.

d) Isotropic temperature factors only.

TABLE 2. Forsterite positional parameters, isotropic temperature factors, and r. m. s. equivalents

Atom	Para-meter	HCP[a]	P = 1 atm						T = 23°C			
			-196°C	23°C	-350°C[b]	-675°C[b]	-1000°C[b]	1020°C	20kb	40 kb	50kb	1 atm after high P
M(1)	X	0	0	0	0	0	0	0	0	0	0	0
	Y	0	0	0	0	0	0	0	0	0	0	0
	Z	0	0	0	0	0	0	0	0	0	0	0
	B		0.09(2)[c]	0.26(1)	0.67(3)	1.20(4)	1.77(4)	1.8(3)	0.16(9)	0.37(9)	0.2(1)	0.43(2)
	ū		0.034	0.057	0.092	0.122	0.150	0.15	0.046	0.069	0.05	0.074
M(2)	X	0	0.9914(3)	0.9915(2)	0.9915(5)	0.9919(5)	0.9924(4)	0.991(3)	0.992(1)	0.991(1)	0.993(1)	0.9914(3)
	Y	1/4	0.2772(1)	0.2774(1)	0.2780(2)	0.2785(2)	0.2772(1)	0.280(1)	0.277(1)	0.280(1)	0.283(1)	0.2771(1)
	Z	1/4	1/4	1/4	1/4	1/4	1/4	1/4	1/4	1/4	1/4	1/4
	B		0.08(2)	0.22(1)	0.66(4)	1.19(4)	1.70(4)	1.8(3)	0.37(10)	0.52(10)	0.6(1)	0.43(2)
	ū		0.031	0.053	0.091	0.122	0.147	0.15	0.069	0.081	0.087	0.074
Si	X	3/8	0.4261(2)	0.4262(1)	0.4257(4)	0.4257(3)	0.4263(3)	0.427(2)	0.427(1)	0.426(1)	0.428(1)	0.4262(2)
	Y	0.0833	0.0939(1)	0.0940(1)	0.0939(2)	0.0941(1)	0.0943(1)	0.094(1)	0.095(1)	0.093(1)	0.101(1)	0.0989(1)
	Z	1/4	1/4	1/4	1/4	1/4	1/4	1/4	1/4	1/4	1/4	1/4
	B		-0.02(2)	0.08(1)	0.33(3)	0.66(3)	0.97(3)	1.0(2)	0.37(8)	0.45(7)	0.7(1)	0.27(1)
	ū		0.00	0.031	0.065	0.091	0.111	0.11	0.069	0.075	0.094	0.058
O(1)	X	3/4	0.7661(6)	0.7657(3)	0.7657(10)	0.7637(9)	0.7631(8)	0.737(2)	0.771(2)	0.768(2)	0.776(2)	0.7664(5)
	Y	0.0833	0.0919(3)	0.0913(2)	0.0910(5)	0.0906(4)	0.0914(4)	0.088(2)	0.092(2)	0.097(2)	0.103(3)	0.0908(3)
	Z	1/4	1/4	1/4	1/4	1/4	1/4	1/4	1/4	1/4	1/4	1/4
	B		0.12(4)	0.26(2)	0.70(6)	1.12(7)	1.51(6)	1.0(5)	-0.1(2)	0.1(2)	0.1(2)	0.43(4)
	ū		0.039	0.057	0.094	0.119	0.137	0.11	0.0	0.035	0.036	0.074
O(2)	X	1/4	0.2202(6)	0.2215(4)	0.2178(9)	0.2178(9)	0.2178(8)	0.224(4)	0.227(2)	0.228(2)	0.228(3)	0.2209(5)
	Y	0.4167	0.4469(3)	0.4474(2)	0.4492(5)	0.4497(4)	0.4497(4)	0.458(3)	0.447(2)	0.444(2)	0.440(3)	0.4478(2)
	Z	1/4	1/4	1/4	1/4	1/4	1/4	1/4	1/4	1/4	1/4	1/4
	B		0.06(4)	0.24(2)	0.60(6)	1.02(7)	1.40(6)	1.0(5)	0.0(2)	0.0(2)	0.4(2)	0.37(3)
	ū		0.026	0.055	0.087	0.113	0.133	0.11	0.0	0.0	0.07	0.069
O(3)	X	1/4	0.2777(4)	0.2777(2)	0.2822(6)	0.2822(6)	0.2843(5)	0.275(3)	0.278(2)	0.276(2)	0.281(2)	0.2784(4)
	Y	0.1667	0.1628(2)	0.1628(1)	0.1619(3)	0.1619(3)	0.1629(3)	0.160(2)	0.162(2)	0.158(2)	0.153(2)	0.1620(2)
	Z	0	0.0333(3)	0.0331(2)	0.0347(6)	0.0352(5)	0.0359(5)	0.030(3)	0.037(1)	0.035(1)	0.032(1)	0.0341(3)
	B		0.07(3)	0.28(2)	0.65(4)	1.15(5)	1.67(5)	1.8(4)	0.2(1)	0.4(1)	0.6(2)	0.41(2)
	ū		0.029	0.060	0.090	0.120	0.144	0.15	0.05	0.07	0.087	0.072

a) "Ideal" hexagonal close-packed olivine model (see Fig. 1).

b) Data of Smyth and Hazen (1973).

c) Parenthesized figures refer to the esd of least units cited.

Linear and volume thermal expansion of pure forsterite as determined by Smyth and Hazen (1973) from 23° to 900°C (Table 1b) and this study (Table 1a) from −196° to 1105°C, are illustrated in Figures 2 and 3. Data of Skinner (1962) on expansion of a synthetic iron-bearing forsterite ($Fo_{96}Fa_{04}$) from 25° to 1127°C are also presented on these graphs. The data of Skinner and this study are in close agreement with respect to the rate of thermal expansion; all expansion curves are essentially parallel over the temperature range 25° to 1100°C. However, serious discrepancies exist between the data of these two studies and those recorded by Smyth and Hazen (1973). The temperature measurements of Skinner and of this study were made with calibrated thermocouples, and reported temperatures are based on these calibrations. However, the thermocouple employed by Smyth and Hazen was not calibrated. The technique of mounting a crystal directly on the thermocouple Pt/Pt–Rh join requires a larger wire diameter (0.150 mm vs. 0.050 mm), and significantly larger join bead (diameter = 0.30 mm vs. 0.075 mm) than that used in the silica capillary mount of this study. Calibration of similar large thermocouples by T. L. Grove and this author revealed that in all cases the measured temperature was *lower* than the real temperature, and that such errors may exceed 100°C at 1000°C (in one experiment, gold of melting point 1063°C appeared to melt at ≈ 950°C). These errors are assumed to reflect the rapid conduction of heat away from the large thermocouple join. Such an error in thermocouple readings could explain the differences between the different sets of cell parameters. If this is the case, then the forsterite refinements reported in Smyth and Hazen (1973) were made at ≈350°, ≈675°, and ≈1000°C. This would explain the deviations in unit-cell parameters at high temperatures, as well as the similarity between Smyth and Hazen's 900°C refinement and the partial 1020°C refinement of this study. In the remainder of this study Smyth and Hazen's data will be assumed to have been obtained at the higher temperatures.

Bond distances

Bond distances and bond angles are tabulated in Tables 4 and 5 respectively. Figure 4 illustrates the variation of average Mg–O bond distances for the two different magnesium octahedra, as well as the

TABLE 3. Forsterite anisotropic temperature factor coefficients[a]

Atom	ij of β_{ij}	-196°C	23°C	~ 350°C	~ 675°C	~ 1000°C	23°C after high pressure
M(1)	11	0.2(4)[b]	2.4(3)	7.5(2)	10.7(4)	15.4(3)	4.2(3)
	22	0.5(1)	1.02(6)	2.1(2)	3.9(2)	5.9(3)	1.26(9)
	33	0.2(3)	1.0(2)	2.9(3)	6.8(4)	9.2(6)	2.7(3)
	12	0.2(2)	0.1(1)	-0.1(1)	-0.2(2)	-0.4(1)	0.0(3)
	13	-0.1(3)	-0.3(2)	-0.5(2)	-1.0(2)	-1.7(3)	-0.2(3)
	23	-0.2(1)	-0.3(1)	-0.7(2)	-1.2(1)	-1.7(2)	-0.3(1)
M(2)	11	0.1(5)	2.2(3)	8.1(8)	12.4(1.0)	18.3(1.5)	4.6(5)
	22	0.4(1)	0.6(1)	1.4(1)	2.7(2)	3.8(4)	1.1(1)
	33	0.4(3)	1.6(2)	4.5(4)	9.1(7)	12.2(1.0)	2.9(3)
	12	-0.0(2)	0.0(1)	0.05(9)	0.2(2)	0.5(3)	0.2(2)
Si	11	-1.8(3)[c]	0.8(2)	2.6(2)	3.8(4)	6.8(5)	1.8(3)
	22	0.2(1)	0.43(4)	1.0(1)	1.8(2)	2.7(4)	0.8(1)
	33	0.2(2)	0.8(1)	2.5(4)	5.9(4)	7.7(7)	2.1(2)
	12	0.1(1)	0.05(8)	0.1(1)	0.3(2)	0.4(2)	0.0(1)
O(1)	11	-0.2(9)[c]	0.9(5)	9.4(1.0)	9.8(1.1)	11.8(1.8)	3.7(9)
	22	0.5(2)	0.9(1)	1.2(2)	2.8(4)	4.3(4)	1.3(2)
	33	1.1(6)	2.3(3)	5.1(7)	8.8(9)	10.8(1.2)	2.7(5)
	12	0.5(4)	0.2(2)	0.3(2)	0.9(1)	4.6(4)	0.3(4)
O(2)	11	-0.2(9)[c]	2.4(5)	7.3(7)	10.0(1.0)	13.5(1.1)	4.2(9)
	22	0.1(2)	0.7(1)	1.4(2)	2.4(3)	3.2(4)	0.8(2)
	33	0.8(5)	2.2(3)	4.0(4)	7.8(6)	10.6(7)	2.6(5)
	12	0.0(4)	0.1(2)	-0.1(2)	-0.1(1)	0.0(2)	0.3(4)
O(3)	11	-0.2(6)[c]	2.2(3)	8.2(9)	11.2(1.1)	16.3(1.4)	3.9(6)
	22	0.4(1)	0.93(7)	1.6(2)	3.0(2)	4.5(3)	1.2(1)
	33	0.2(4)	1.6(2)	3.7(4)	8.0(7)	10.3(1.2)	2.8(4)
	12	0.0(2)	0.1(1)	-0.3(1)	-0.5(1)	-0.3(1)	-0.0(2)
	13	0.3(4)	-0.3(2)	-0.2(1)	-0.5(3)	-0.5(2)	0.0(4)
	23	0.0(2)	0.4(1)	0.6(2)	1.2(2)	1.9(2)	0.3(2)

a) $\beta_{ij} \times 10^3$: for M(2), Si, O(1) and O(2) $\beta_{13} = \beta_{23} = 0$.

b)   Parenthesized figures refer to the esd of least units cited.

c)   Atom is non-positive definite.

average Si–O tetrahedral bond distance. The bond expansion curve of the $M(1)$ octahedron is remarkably similar to that of Mg–O in periclase. As discussed in Hazen (1976), periclase Mg–O bonds have an absolute zero bond length of 2.10 Å. They expand at an increasing rate to a temperature of approximately 450 K, and above this temperature Mg–O bonds have a relatively constant expansion rate of about 2.7×10^{-5}Å/K. Forsterite Mg(1)–O bonds have an absolute-zero mean bond distance of ≈2.09 Å. They expand at an increasing rate to approximately 400 K, and above this temperature expand at a constant rate of 2.8×10^{-5}Å/K. The longer Mg(2)–O forsterite average bond distance has qualitatively similar expansion characteristics. The absolute-zero bond distance for Mg(2)–O is ≈2.13 Å, and above 450 K a constant expansion of 3.4×10^{-5} Å/K was observed. It appears from these average bond data for magnesium-to-oxygen bonds in periclase and forsterite that longer bonds may have a higher rate of

thermal expansion. To test this possibility all individual magnesium–oxygen bonds have been plotted versus temperature in Figure 5. While there is some scatter in these data, longer Mg–O bonds show significantly higher rates of thermal expansion (as much as four times greater) than shorter bonds, as illustrated in Figure 6. This fact is consistent with the theory that shorter bonds are stronger bonds.

Analysis of the silicon–oxygen bonds in forsterite versus temperature is less straightforward. The average Si–O bond length is constant or increases only slightly from liquid-nitrogen temperature to room temperature, as illustrated in Figure 4. The distance is seen to decrease by over 0.5 percent between 300 K and 800 K; only above 1000 K does the average Si–O bond appear to expand. This unexpected behavior of forsterite Si–O bonds between −196° and 1000°C cannot be explained with a simple bonding model of Si–O alone. Rather, complex Mg–O–Si interactions must be considered before a thorough understanding
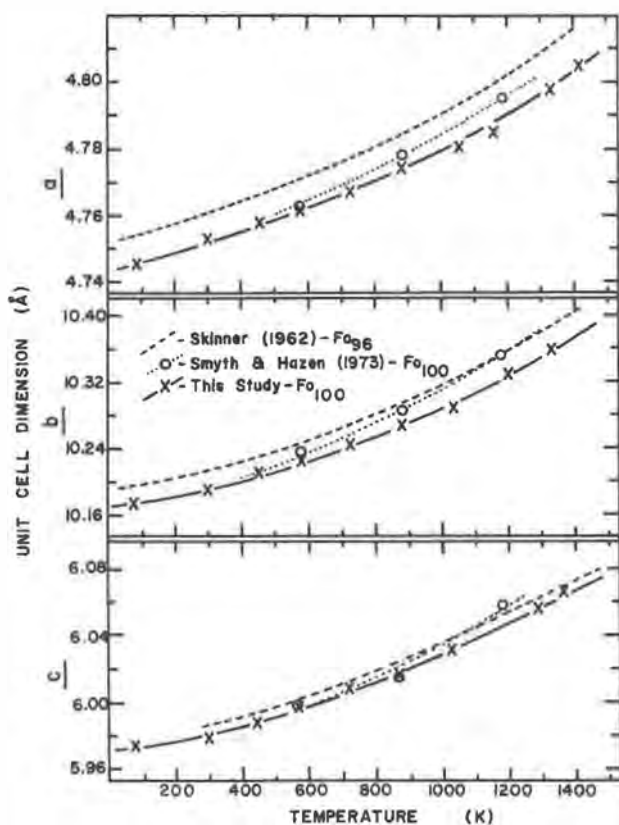
FIG. 2. Forsterite unit-cell dimensions versus temperature. Data of Smyth and Hazen (1973) have not been corrected for presumed errors in temperature.
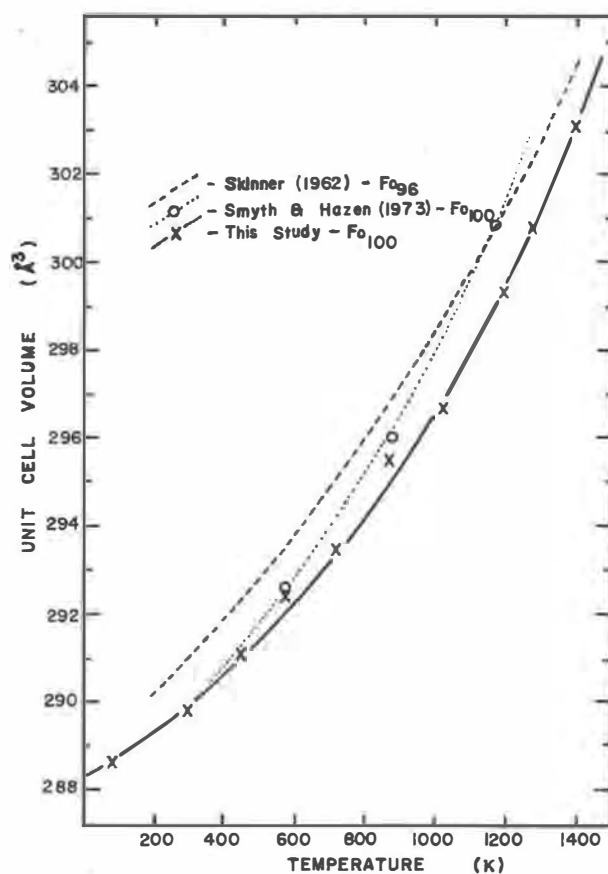

FIG. 3. Forsterite unit-cell volume versus temperature. Data of Smyth and Hazen (1973) have not been corrected for presumed errors in temperature.

of Si–O bond distance variation in forsterite can be achieved.

The variation between individual Si–O bonds with temperature is illustrated in Figure 7. Silicon-to-oxygen bonds in forsterite provide a striking example of the greater thermal response of longer bonds. The shortest Si–O(1) bond shows no variation in length between $-196°$ and $1000°C$, while the longest Si–O(2) bond shows a maximum variation of 1.3 percent over this range.

An important and often neglected aspect of bond distance analysis is the effect of thermal vibrations on mean interatomic separation. Interatomic distances

reported in most studies (including this one) are calculated as the distance between mean atomic positions. However, Busing and Levy (1964) and Smyth (1973) have demonstrated that a better measure of interatomic distance is the *mean* separation. In general, when thermal vibrations are large, the mean separation of two atoms will be greater than the separation of atomic positions. Thus, bond thermal expansion based on mean separation may be greater, and may represent a more valid physical situation, than that reported in most studies which quote distance between atomic coordinates.

It will prove useful to analyze thermally-corrected bond distances for Si–O in forsterite as an illustration of the possible magnitudes of thermal bond distance corrections. Lower, upper, riding, noncorrelated, and uncorrected bond distances were computed by the least-squares and errors programs (RFINE and BAD-TEA, Finger, 1969). These data for the mean Si–O bond distance in forsterite are tabulated for temperatures from $-196°$ to $1000°C$ in Table 4, and are

TABLE 4. Thermally corrected mean separation of Si–O in forsterite (Å)

$T(°C)$	Centroid separation	Lower bound	Riding	Non-correlated	Upper Bound
-196	1.633	1.633	1.633	1.634	1.635
23	1.630	1.630	1.631	1.633	1.636
350	1.625	1.625	1.627	1.632	1.640
675	1.624	1.624	1.627	1.638	1.652
1000	1.630	1.630	1.635	1.651	1.665

TABLE 5. Forsterite bond distances[a]

Bond [Multiplicity]		P = 1 atm						T = 23°C			
		23°C	-196°C	-350°C[b]	-675°C[b]	-1000°C[b]	1020°C	20 kb	40 kb	50 kb	1 atm (after high P)
Si Tetrahedron											
Si-O(1)	[1]	1.615(3)[c]	1.616(2)	1.614(3)	1.615(5)	1.615(4)	1.53(2)	1.63(1)	1.62(1)	1.64(1)	1.617(3)
Si-O(2)	[1]	1.640(3)	1.649(2)	1.636(4)	1.636(5)	1.649(4)	1.60(2)	1.66(2)	1.66(2)	1.76(2)	1.645(3)
Si-O(3)	[2]	1.633(2)	1.633(2)	1.624(3)	1.623(3)	1.628(3)	1.67(2)	1.60(1)	1.60(1)	1.56(1)	1.625(2)
mean Si-O		1.630	1.633	1.625	1.624	1.630	1.62	1.62	1.62	1.63	1.628
O(1)-O(2)	[1]	2.725(6)	2.740(4)	2.720(6)	2.719(6)	2.733(6)	2.60(3)	2.78(2)	2.80(2)	2.84(1)	2.736(4)
O(1)-O(3)	[2]	2.744(5)	2.753(4)	2.742(5)	2.740(5)	2.739(4)	2.80(3)	2.75(1)	2.73(1)	2.71(1)	2.752(3)
O(2)-O(3)[d]	[2]	2.558(5)	2.550(3)	2.537(5)	2.538(5)	2.561(5)	2.50(3)	2.51(3)	2.50(3)	2.49(2)	2.537(3)
O(3)-O(3)[d]	[1]	2.590(7)	2.590(4)	2.587(6)	2.589(7)	2.595(6)	2.66(3)	2.53(1)	2.55(1)	2.59(1)	2.581(4)
mean O-O		2.653	2.656	2.644	2.644	2.655	2.64	2.63	2.63	2.64	2.649
M(1) Octahedron											
M(1)-O(1)	[2]	2.083(2)	2.085(1)	2.091(3)	2.101(3)	2.117(3)	2.17(2)	2.06(1)	2.08(1)	2.09(1)	2.079(2)
M(1)-O(2)	[2]	2.074(2)	2.069(1)	2.080(3)	2.087(3)	2.097(3)	2.06(1)	2.04(1)	2.04(1)	2.05(2)	2.068(2)
M(1)-O(3)	[2]	2.145(3)	2.126(2)	2.140(3)	2.153(3)	2.180(3)	2.13(2)	2.11(1)	2.07(2)	2.03(2)	2.126(2)
mean M(1)-O		2.101	2.095	2.104	2.113	2.131	2.12	2.07	2.06	2.06	2.091
O(1)-O(3)[e]	[2]	2.864(5)	2.846(4)	2.871(5)	2.890(5)	2.911(5)	3.00(2)	2.81(3)	2.79(1)	2.76(3)	2.848(3)
O(1)-O(3')	[2]	3.122(1)	3.104(4)	3.109(5)	3.123(5)	3.160(5)	3.12(2)	3.09(3)	3.07(4)	2.95(3)	3.094(3)
O(1)-O(2)[e]	[2]	2.863(6)	2.849(4)	2.861(6)	2.870(6)	2.888(6)	2.90(2)	2.80(2)	2.83(2)	2.88(2)	2.839(4)
O(1)-O(2')	[2]	3.027(1)	3.022(3)	3.036(3)	3.050(3)	3.067(3)	3.07(6)	3.01(1)	3.00(1)	3.02(1)	3.022(1)
O(2)-O(3')	[2]	3.342(2)	3.341(3)	3.373(3)	3.380(2)	3.388(4)	3.37(2)	3.31(2)	3.26(2)	3.24(2)	3.339(2)
O(2)-O(3)[d]	[2]	2.558(5)	2.550(3)	2.537(5)	2.538(5)	2.561(5)	2.50(3)	2.51(3)	2.50(3)	2.49(2)	2.537(3)
mean O-O		2.963	2.952	2.965	2.975	2.996	2.99	2.92	2.91	2.89	2.947
M(2) Octahedron											
M(2)-O(1)	[1]	2.166(3)	2.166(4)	2.199(5)	2.219(6)	2.237(5)	2.32(3)	2.14(2)	2.12(1)	2.06(3)	2.179(3)
M(2)-O(2)	[1]	2.045(5)	2.040(3)	2.057(5)	2.066(5)	2.068(5)	2.13(3)	2.04(2)	2.00(2)	1.92(2)	2.053(3)
M(2)-O(3)	[2]	2.208(4)	2.208(3)	2.231(4)	2.245(4)	2.258(3)	2.28(2)	2.19(1)	2.22(1)	2.27(2)	2.214(2)
M(2)-O(3")	[2]	2.064(4)	2.066(2)	2.073(3)	2.082(4)	2.086(3)	2.08(2)	2.08(1)	2.07(1)	2.06(3)	2.072(2)
mean M(2)-O		2.126	2.126	2.144	2.156	2.165	2.19	2.12	2.11	2.11	2.134
O(1)-O(3")	[2]	3.008(5)	3.016(4)	3.052(5)	3.074(5)	3.080(5)	3.07(2)	3.01(3)	2.98(3)	3.07(4)	3.022(1)
O(1)-O(3)[e]	[2]	2.864(5)	2.846(4)	2.871(5)	2.890(5)	2.911(5)	3.00(2)	2.81(3)	2.79(1)	2.76(1)	2.848(4)
O(2)-O(3)	[2]	3.177(5)	3.120(4)	3.224(5)	3.247(5)	3.257(5)	3.26(2)	3.15(3)	3.14(3)	3.24(1)	3.197(3)
O(2)-O(3''')	[2]	2.926(5)	2.920(3)	2.923(5)	2.933(5)	2.947(4)	3.00(3)	2.94(1)	2.92(1)	2.85(1)	2.926(3)
O(3)-O(3)[d]	[1]	2.590(7)	2.590(4)	2.587(6)	2.589(7)	2.595(6)	2.66(3)	2.53(1)	2.55(1)	2.59(1)	2.581(4)
O(3)-O(3")	[2]	2.975(4)	2.990(3)	3.014(4)	3.029(4)	3.031(4)	3.05(2)	3.02(3)	3.03(2)	3.07(3)	3.005(2)
O(3")-O(3")	[1]	3.393(2)	3.386(3)	3.412(2)	3.432(2)	3.465(2)	3.39(2)	3.39(1)	3.42(1)	3.64(1)	3.398(3)
mean O-O		2.990	2.980	3.014	3.031	3.043	3.07	2.98	2.97	3.02	2.998
O(1) Tetrahedron											
O(1)-M(1)[B]	[2]	2.083(2)	2.085(1)	2.091(3)	2.101(3)	2.117(3)	2.17(2)	2.06(1)	2.08(1)	2.09(1)	2.079(2)
O(1)-M(2)[B]	[1]	2.166(3)	2.166(4)	2.199(5)	2.219(6)	2.237(5)	2.32(3)	2.14(2)	2.12(1)	2.06(3)	2.179(3)
O(1)-Si[A]	[1]	1.615(3)	1.616(2)	1.614(5)	1.615(5)	1.615(4)	1.53(2)	1.63(1)	1.62(1)	1.64(1)	1.617(3)
mean O(1)-M		1.987	1.988	1.999	2.009	2.022	2.05	1.97	1.97	1.97	1.989
M(1)[B]-M(1)[B]	[1]	2.993(1)	2.988(3)	3.000(3)	3.014(3)	3.030(3)	3.033(3)	2.977(3)	2.970(3)	2.97(1)	2.989(1)
M(1)[B]-M(2)[B]	[2]	3.197(2)	3.192(3)	3.217(3)	3.238(3)	3.267(3)	3.28(1)	3.17(1)	3.17(1)	3.18(1)	3.196(1)
M(1)[B]-Si[A]	[2]	3.256(2)	3.250(3)	3.264(3)	3.276(3)	3.288(3)	3.29(1)	3.244(5)	3.23(1)	3.243(6)	3.253(2)
M(2)[B]-Si[A]	[1]	3.249(3)	3.247(3)	3.260(4)	3.270(4)	3.283(4)	3.28(2)	3.23(2)	3.16(1)	3.19(1)	3.251(2)
O(2) Tetrahedron											
O(2)-M(1)[B]	[2]	2.074(2)	2.069(1)	2.080(3)	2.087(3)	2.097(3)	2.06(1)	2.04(1)	2.04(1)	2.05(2)	2.068(2)
O(2)-M(2)[A]	[1]	2.045(5)	2.040(3)	2.057(5)	2.066(5)	2.068(5)	2.13(3)	2.04(2)	2.00(2)	1.92(2)	2.053(3)
O(2)-Si[B]	[1]	1.640(3)	1.649(2)	1.636(4)	1.636(5)	1.649(4)	1.60(2)	1.66(2)	1.66(2)	1.76(2)	1.645(3)
mean O(2)-M		1.958	1.957	1.963	1.969	1.978	1.96	1.95	1.94	1.94	1.959
M(1)[B]-M(1)[B]	[1]	2.993(1)	2.988(3)	3.000(3)	3.014(3)	3.030(3)	3.033(3)	2.977(3)	2.970(3)	2.97(1)	2.989(1)
M(1)[B]-M(2)[A]	[2]	3.637(2)	3.633(2)	3.645(3)	3.654(3)	3.665(3)	3.68(1)	3.617(7)	3.59(7)	3.55(2)	3.632(2)
M(1)[B]-Si[B]	[2]	2.692(2)	2.690(2)	2.699(2)	2.710(2)	2.725(2)	2.73(1)	2.687(6)	2.671(6)	2.70(1)	2.693(1)
M(2)[A]-Si[B]	[1]	3.283(2)	3.278(3)	3.289(3)	3.302(4)	3.309(5)	3.32(2)	3.26(1)	3.26(1)	3.21(1)	3.280(1)
O(3) Tetrahedron											
O(3)-M(1)[B]	[1]	2.145(3)	2.126(2)	2.140(3)	2.153(3)	2.180(3)	2.13(2)	2.11(1)	2.07(2)	2.03(2)	2.126(2)
O(3)-M(2)[B]	[1]	2.205(4)	2.208(3)	2.231(4)	2.245(4)	2.258(3)	2.28(2)	2.19(1)	2.22(1)	2.27(2)	2.214(2)
O(3)-M(2)[A]	[1]	2.064(4)	2.066(2)	2.073(3)	2.082(4)	2.086(3)	2.08(2)	2.08(1)	2.07(1)	2.06(3)	2.072(2)
O(3)-Si[B]	[1]	1.633(2)	1.633(2)	1.624(3)	1.623(3)	1.628(3)	1.67(2)	1.60(1)	1.60(1)	1.56(1)	1.625(2)
mean O(3)-M		2.012	2.008	2.017	2.026	2.038	2.04	2.00	1.99	1.98	1.987
M(1)[B]-M(2)[B]	[1]	3.197(2)	3.192(3)	3.217(3)	3.238(3)	3.267(3)	3.28(1)	3.17(1)	3.17(1)	3.18(1)	3.196(1)
M(1)[B]-M(2)[A]	[1]	3.579(2)	3.579(3)	3.592(3)	3.603(2)	3.617(2)	3.61(1)	3.565(9)	3.53(1)	3.51(2)	3.580(2)
M(1)[B]-Si[B]	[1]	2.692(2)	2.690(2)	2.699(2)	2.710(2)	2.725(2)	2.73(1)	2.687(6)	2.671(6)	2.70(1)	2.693(1)
M(2)[B]-M(2)[A]	[1]	3.862(4)	3.856(3)	3.872(3)	3.886(3)	3.912(3)	3.91(2)	3.845(2)	3.844(2)	3.85(1)	3.858(4)
M(2)[B]-Si[B]	[1]	2.783(3)	2.781(3)	2.797(3)	2.811(3)	2.829(3)	2.84(2)	2.77(1)	2.78(1)	2.73(1)	2.790(2)
M(2)[A]-Si[B]	[1]	3.282(2)	3.278(3)	3.288(3)	3.303(4)	3.311(5)	3.32(2)	3.25(1)	3.25(1)	3.20(1)	3.263(2)

a) All distances in Å. b) Data of Smyth and Hazen (1973).

c) Parenthesized figures refer to the esd of least units cited. d) Edge shared between an octahedron and tetrahedron.
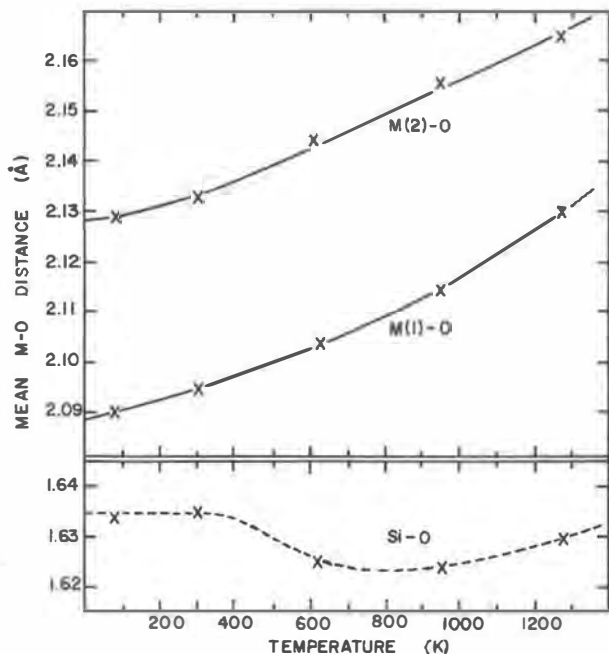
e) Edge shared between two octahedra.

FIG. 4. Forsterite Mg–O and Si–O mean bond distances versus temperature.

FIG. 6. Forsterite Mg–O bond length thermal expansion versus 0 Kelvin Mg–O distance. 0 K Mg–O distance is extrapolated from Fig. 5.

plotted in Figure 8. From Figure 8 it is evident that uncorrected, lower bound, and riding corrections behave in a similar way, and are not significantly different from each other. Thus, if metal-oxygen bonds have predominantly parallel correlated vibration mo-
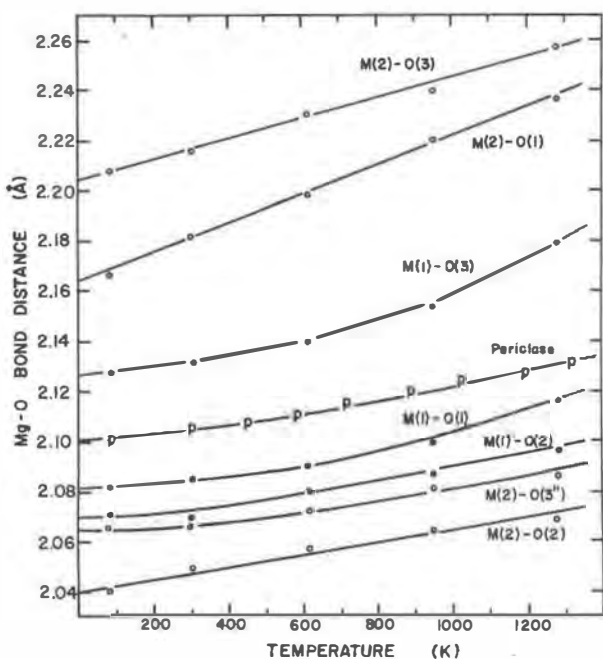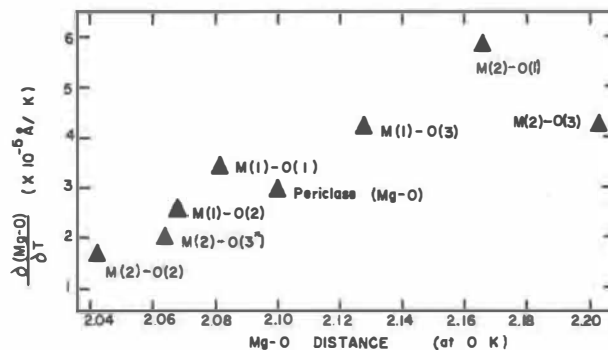
tion, then the uncorrected distance usually reported is a valid measure of the physical separation of atoms. However, non-correlated and anti-correlated (upper bound) separations are significantly larger than the lower bound, and may give a totally different picture of bond distances and thermal expansion at elevated temperature. If a bond has a large component of anti-parallel or noncorrelated vibrations, the simple centroid separation distance will not provide a realistic measure of mean atomic separation. It should be recognized that reported bond distances and bond thermal expansions represent the lower limits of these physical quantites.

Temperature factors

Isotropic temperature factors of the six atoms in forsterite's asymmetric unit are plotted versus temperature in Figure 9. All six curves show the same general form of a near-zero slope at 0 K, a rapidly increasing slope between 0 and 500 K, and an approximately constant slope above 500 K. This is the same behavior as that recorded for periclase (Hazen, 1976). Also, as with periclase, magnesium and oxygen atoms have approximately equal magnitudes of thermal vibrations. However, silicon's isotropic tem-
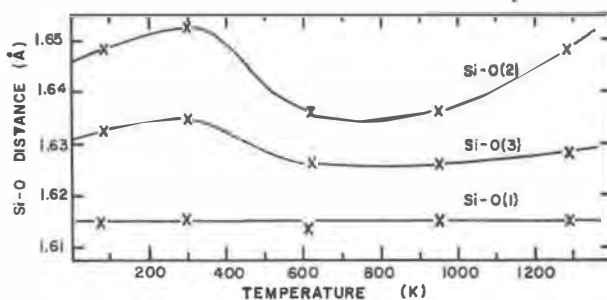

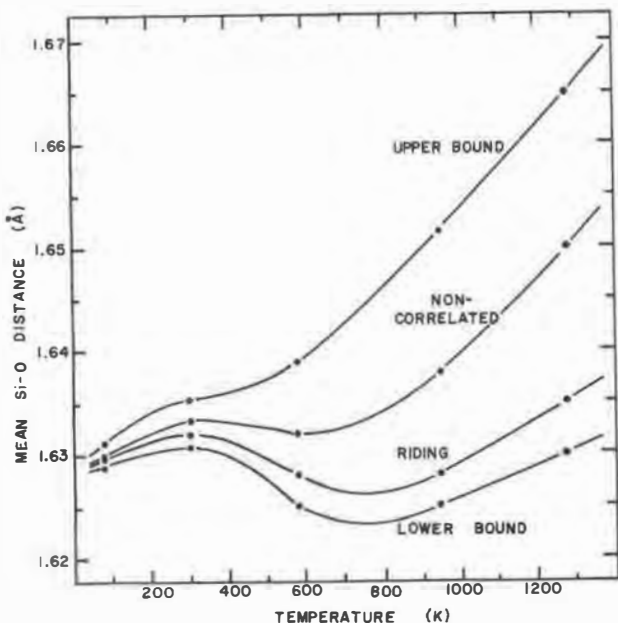FIG. 5. Forsterite individual Mg–O bond distance versus temperature.

FIG. 7. Forsterite individual Si–O bond distances versus temperature.

Fig. 8. Forsterite Si–O mean distances versus temperature corrected for several thermal-motion models.

Fig. 9. Forsterite isotropic temperature factors versus temperature.

perature factor is only about half that of the magnesium and oxygen atoms. This behavior has been observed in many other silicates (Burnham, 1965), and is a consequence of the strong bonds between oxygen and four-valent silicon.

L. Finger (personal communication) has noted a possible source of error in the magnitudes of temperature factors reported in this study. No corrections were made for secondary extinction; when a gem quality crystal such as synthetic forsterite is used
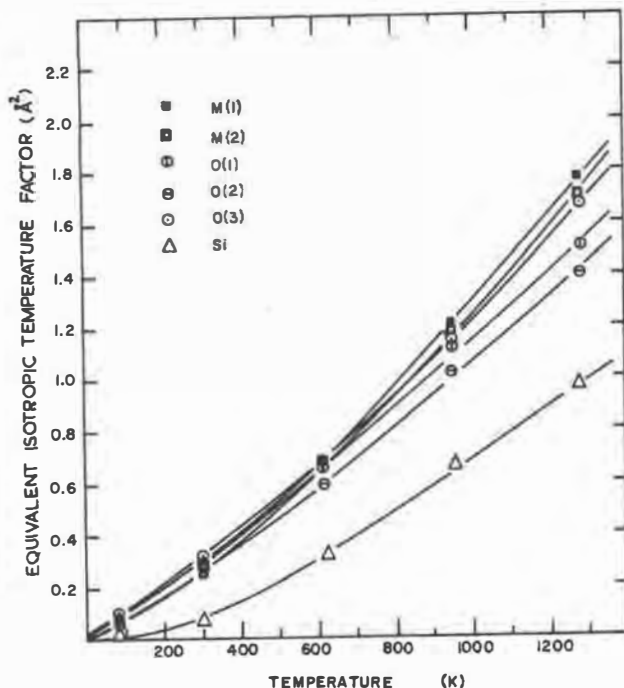
several strong reflections with $|F_{obs}| \ll |F_{calc}|$ are rejected from the data set. Consequently, the scale factor will be too high, and the temperature factors will be too low. This effect explains the nonpositive-definite thermal factors of oxygen and silicon in the liquid-nitrogen temperature case (see Table 3). Thus, while the qualitative aspects of Figure 9 are correct, the absolute values reported may be low.

TABLE 6.   Forsterite bond angles

| Angle [Multiplicity] | | HCP[a] | $\bar{P}$ = 1 atm | | | | | | T = 23°C | | | |
			23°C	-196°C	-350°C[c]	-675°C[c]	-1000°C[c]	1020°C	20 kb	40 kb	50 kb	After high P 1 atm
O(1)-Si-O(2)	[1]	109.5	114.1(3)[b]	114.2(2)	113.7(2)	113.6(2)	113.7(2)	114(1)	115.1(1.0)	115.7(6)	115(1)	114.1(2)
O(1)-Si-O(3)	[2]	109.5	115.6(2)	115.9(1)	115.7(1)	115.6(1)	115.2(1)	117(1)	116.5(5)	117.4(1.1)	116(1)	116.1(1)
O(2)-Si-O(3)	[2]	109.5	102.7(2)	102.0(1)	102.2(1)	102.3(2)	102.8(1)	99(1)	100.9(7)	100.0(7)	97(1)	101.7(1)
O(3)-Si-O(3')	[1]	109.5	104.6(3)	105.0(2)	105.6(2)	105.9(2)	105.7(2)	106(1)	104.6(9)	105.7(6)	110(1)	105.1(1)
mean O-Si-O		109.5	109.2	109.1	109.2	109.2	109.2	109	109.1	109.4	109	109.1
O(1)-M(1)-O(3)	[2]	90	85.1(2)	85.0(1)	85.4(1)	85.6(2)	85.3(1)	87(6)	84.5(6)	84.5(6)	83.8(8)	85.3(1)
O(1)-M(1)-O(3')	[2]	90	94.9(2)	95.0(1)	94.6(1)	94.4(2)	94.7(1)	91(1)	95.5(6)	95.5(6)	96.2(8)	94.7(1)
O(1)-M(1)-O(2)	[2]	90	86.8(1)	86.6(1)	86.6(1)	86.5(1)	86.6(1)	88(1)	85.8(4)	86.7(4)	86.7(4)	86.4(1)
O(1)-M(1)-O(2')	[2]	90	93.2(1)	93.4(1)	93.4(1)	93.5(1)	93.4(1)	93(1)	94.2(4)	93.3(4)	93.3(4)	93.5(1)
O(2)-M(1)-O(3')	[2]	90	105.4(2)	105.2(1)	106.1(1)	106.5(2)	106.5(1)	107(1)	105.7(7)	105.2(7)	104.9(7)	105.6(1)
O(2)-M(1)-O(3)	[2]	90	74.6(2)	74.8(1)	73.9(1)	73.5(2)	73.5(1)	73(1)	74.3(7)	74.8(7)	75.1(7)	74.4(1)
mean O-M(1)-O		90	90	90	90	90	90	90	90	90	90	90
O(1)-M(2)-O(3")	[2]	90	90.3(1)	90.9(1)	91.1(1)	91.2(1)	90.8(1)	90(1)	91.2(6)	90.9(6)	92(1)	91.2(1)
O(1)-M(2)-O(3)	[2]	90	81.7(1)	81.1(1)	80.8(1)	80.7(1)	80.7(1)	81(1)	80.8(7)	80.2(7)	79(1)	80.8(1)
O(2)-M(2)-O(3)	[2]	90	96.7(2)	96.9(1)	97.4(2)	97.7(2)	97.6(1)	99(1)	96.2(6)	96.2(6)	97(1)	97.0(1)
O(2)-M(2)-O(3''')	[2]	90	90.8(1)	90.6(1)	90.1(1)	90.0(1)	90.4(1)	90(1)	91.0(7)	91.6(7)	91.5(1.0)	90.3(1)
O(3)-M(2)-)(3')	[1]	90	71.9(2)	71.8(1)	70.9(2)	70.4(2)	70.1(2)	72(1)	70.6(6)	70.1(6)	69.4(7)	71.3(1)
O(3)-M(2)-O(3")	[2]	90	88.3(1)	88.7(1)	88.8(2)	88.8(1)	88.4(1)	89(1)	89.1(4)	89.6(4)	90.0(7)	89.0(1)
O(3)-M(2)-O(3''')	[1]	90	110.7(2)	110.0(1)	110.8(1)	111.3(2)	112.3(2)	109(1)	110.6(6)	109.9(6)	109.7(6)	110.1(1)
mean O-M(2)-O		90	89.9	89.9	89.8	89.9	89.9	90	89.8	89.8	90	89.9

a) "Ideal" hexagonal close-packed olivine model (see Fig. 1).

b) Parenthesized figures refer to the esd of least units cited.

c) Data of Smyth and Hazen (1973).

Because each of olivine's six atoms has an irregular coordination polyhedron, anisotropic vibrations are expected, and have been modeled as triaxial ellipsoids in the refinement procedures. Anisotropic temperature factors are presented in Table 3, while corresponding magnitudes and orientations of thermal ellipsoids appear in Table 7. These values agree with data reported by Brown (1970), and while the magnitudes of thermal ellipsoids increase with temperature, there is no significant change in ellipsoid orientation with changes in temperature.

Data collection: 1 atm to 50 kbar

The forsterite crystal used in the liquid-nitrogen–temperature studies was remounted with the good (010) cleavage parallel to the diamond faces of the miniature pressure cell. The cell was tightened, and unit-cell parameters were determined on the four-circle diffractometer as $a = 4.743 \pm 0.005$, $b = 10.092 \pm 0.010$, $c = 5.954 \pm 0.006$ Å, and volume = 285.0 ± 0.5 Å^3, which represents a volume decrease of 1.65 percent. Pressure calibration was based on a volume compressibility of -7.6×10^{-4}/kbar for olivine as measured by Olinger and Halleck (1975). It thus appears that the first high-pressure data collection was made at approximately 20 kbar. All available diffractions were collected, but of 969 measured intensities only 329 were observed ($I < 2\sigma$). After ten cycles of refinement with isotropic temperature factors, convergence was achieved with a weighted R of 7.0 percent (9.4 percent unweighted). Refinement conditions, atom parameters, and isotropic temper-

TABLE 7. Magnitudes and orientations of forsterite thermal ellipsoids[a]

T(°C)	i of r_i	M(1) r_i	a	b	c	M(2) r_i	a	b	c	SI r_i	a	b	c
-196	1	0.01(2)[b]	12(61)	102(27)	93(134)	0.01(2)	1(14)	89(14)	90				
	2	0.019(13)	95(134)	100(30)	168(39)	0.027(10)	90	90	180				
	3	0.054(5)	101(9)	164(9)	79(10)	0.045(6)	91(14)	1(14)	90				
23	1	0.037(4)	74(10)	76(4)	21(7)	0.051(3)	9(41)	99(41)	90	0.022(7)	3(5)	93(5)	90
	2	0.053(3)	17(10)	99(6)	104(10)	0.054(3)	98(47)	172(47)	90	0.030(3)	90	90	180
	3	0.075(2)	95(5)	164(4)	75(3)	0.055(3)	90	90	0	0.032(3)	87(5)	3(5)	90
-350	1	0.068(6)	80(10)	73(5)	19(7)	0.086(5)	94(23)	4(23)	90	0.054(6)	5(13)	95(13)	90
	2	0.094(5)	10(10)	93(13)	99(10)	0.090(5)	90	90	180	0.067(5)	90	90	180
	3	0.110(4)	91(13)	163(6)	73(6)	0.097(4)	4(23)	86(23)	90	0.073(4)	85(13)	5(13)	90
-675	1	0.101(5)	56(13)	73(5)	39(11)	0.117(5)	49(43)	140(43)	90	0.065(5)	7(6)	97(6)	90
	2	0.115(4)	34(13)	102(6)	121(12)	0.122(5)	140(43)	130(43)	90	0.100(4)	97(6)	173(6)	90
	3	0.149(4)	91(5)	159(6)	69(4)	0.129(4)	90	90	180	0.104(3)	90	90	0
-1000	1	0.117(4)	58(7)	75(2)	37(6)	0.140(4)	53(16)	143(16)	90	0.088(4)	8(4)	98(4)	90
	2	0.140(4)	32(7)	99(4)	121(6)	0.149(4)	144(16)	126(16)	90	0.119(3)	90	90	180
	3	0.185(3)	89(3)	162(2)	72(3)	0.151(4)	90	90	0	0.122(3)	82(4)	8(4)	90
23 (after high pressure)	1	0.066(4)	58(32)	72(13)	37(23)	0.069(4)	36(18)	126(13)	90	0.046(4)	2(9)	92(9)	90
	2	0.071(4)	32(32)	107(16)	116(27)	0.072(3)	90	90	180	0.062(3)	90	90	180
	3	0.084	96(12)	155(10)	66(9)	0.078(4)	54(18)	36(18)	90	0.065(3)	88(9)	2(9)	90

T(°C)	i of r_i	O(1) r_i	a	b	c	O(2) r_i	a	b	c	O(3) r_i	a	b	c
-196													
23	1	0.031(9)	10(8)	100(8)	90	0.048(6)	57(37)	147(37)	90	0.044(4)	48(16)	109(7)	48(13)
	2	0.064(4)	90	90	180	0.055(6)	147(37)	123(37)	90	0.055(4)	42(16)	75(9)	128(14)
	3	0.069(4)	81(8)	10(8)	90	0.062(5)	90	90	0	0.074(3)	88(7)	25(7)	65(6)
-350	1	0.079(11)	80(19)	170(19)	90	0.084(10)	73(62)	17(62)	90	0.073(8)	93(15)	123(13)	34(13)
	2	0.097(9)	90	90	180	0.086(10)	90	90	180	0.094(7)	139(31)	122(26)	113(20)
	3	0.105(9)	10(19)	80(19)	90	0.092(10)	17(62)	107(67)	90	0.103(6)	131(31)	49(23)	67(17)
-675	1	0.101(10)	25(15)	115(15)	90	0.107(9)	7(77)	83(77)	90	0.107(7)	99(48)	132(8)	43(19)
	2	0.127(8)	90	90	180	0.113(9)	96(84)	6(84)	90	0.113(6)	165(29)	94(34)	105(37)
	3	0.128(8)	64(15)	25(15)	90	0.120(8)	90	90	0	0.140(6)	102(10)	42(8)	51(8)
-1000	1	0.116(7)	7(9)	97(9)	90	0.125(7)	1(46)	91(46)	90	0.125(5)	86(19)	121(5)	31(4)
	2	0.142(7)	90	90	180	0.133(7)	91(46)	179(46)	90	0.137(5)	174(13)	96(12)	90(16)
	3	0.154(7)	83(9)	7(9)	90	0.141(7)	90	90	0	0.171(5)	95(6)	32(5)	59(4)
23 (after high pressure)	1	0.063(8)	16(16)	106(16)	90	0.062(8)	51(27)	39(27)	90	0.067(5)	3(156)	88(85)	93(136)
	2	0.071(7)	90	90	180	0.068(7)	90	90	180	0.068(5)	93(158)	59(17)	149(21)
	3	0.085(8)	74(16)	16(16)	90	0.073(7)	39(27)	129(27)	90	0.081(5)	90(16)	31(16)	59(16)

a) All data at 1 atm.

b) Parenthesized figures refer to the esd of least units cited.

c) Atom is non-positive definite.

ature factors are given in Tables 1b and 2 respectively.

The pressure cell was tightened again for a second data collection at higher pressure, but the crystal was crushed and no further experiments were possible on the specimen. Another smaller crystal plate approximately $160 \times 140 \times 80$ μm with (010) cleavage was mounted in the diamond cell, which was tightened as before. Cell dimensions of $a = 4.734 \pm 0.005$, $b = 10.02 \pm 0.01$, $c = 5.940 \pm 0.006$ Å, and volume $= 281.8 \pm 0.5$ Å³, indicated a pressure of approximately 40 kbar. Only 374 of 964 measured diffractions were observed, and these data were refined to an R of 7.3 percent (9.6 percent unweighted) after 10 cycles. The pressure cell was tightened for a third high-pressure data collection; this tightening was stopped when a small fracture was observed in the crystal. Subsequent precession and cone-axis photographs showed that diffraction intensities remained fairly sharp (though some spreading of diffraction peaks was noted), and no change occurred in space group or lattice translations. Unit-cell dimensions of the third high-pressure data collection were $a = 4.712 \pm 0.005$, $b = 9.967 \pm 0.010$, $c = 5.955 \pm 0.006$ Å, and volume 279.7 ± 0.5 Å³, which represents a 3.50 percent volume decrease from 1 atm. At hydrostatic pressure such a volume decrease would imply a pressure of approximately 50 kbar. However, closer examination of cell-edge parameters reveals that while a and b have decreased in length, the c cell dimension increased between the second and third high-pressure data collection. Thus, there is serious doubt that the presumed 50 kbar data collection was made under hydrostatic pressure. It is probable that at this highest pressure the forsterite crystal was in direct contact with the diamonds, and this fact may account for both the small fracture and the anomalous cell parameters of this specimen.

Data collection at ≈ 50 kbar (nonhydrostatic) pressure included 1429 measured reflections of which only 332 were observed. The fact that fewer than 25 percent of measured diffractions were observed may be ascribed in part to absorption of X-rays by the diamond cell. However, a more basic cause is that peak-to-noise ratio was low for all diffraction maxima: peaks were broad, and scattered X-radiation from the pressure cell was high. Thus, while a weighted R of 6.8 percent was obtained for refinement with isotropic temperature factors, the unweighted R was 12.3 percent, indicating a serious lack of precision for the weak observed data.

Further high-pressure data collection was not at-tempted due to the beginning of fracturing in the forsterite crystal. This crystal was removed from the pressure cell and was remounted on a standard go-niometer for a final room-pressure and temperature data collection. Unit-cell parameters of this crystal were remeasured, and found to agree within experi-mental error with earlier determinations (see Table 1). 1026 diffraction intensities were measured and 790 of these were observed and used in least-squares re-finement with anisotropic temperature factors. After 12 cycles of refinement, an unweighted R of 3.9 per-cent was achieved, and all atomic coordinates match those of the original room-temperature and pressure refinement within twice the estimated standard devia-tion, as recorded in Table 2. All observed and calcu-lated structure factors for forsterite are available from the author on request.

Bond distances and angles from refinements using the data collected at high pressures are listed in Ta-bles 5 and 6. The estimated standard deviations of these distances are large, and small changes in bond distances with pressure are thus difficult to detect. However, mean M–O bond lengths for both $M(1)$ and $M(2)$ show compression exceeding 1.0 percent at pressures to 50 kbar, as illustrated in Figure 10. On the other hand, the silicon tetrahedron shows no bond compression with respect to experimental error over the same pressure range. Thus, in olivine, mag-nesium–oxygen bonds appear more compressible than silicon–oxygen bonds.

Isotropic temperature factors show little systematic change with increasing pressure. A slight increase in apparent thermal vibrations with increasing pressure is observed for $M(2)$, Si, $O(2)$, and $O(3)$, but these changes are small, and perhaps insignificant, consid-ering their estimated standard deviations. Significant changes in refined thermal vibration parameters are seen in comparisons of room-temperature and pres-sure forsterite refinements before and after high-pres-sure data collection; average apparent root-mean-square displacements are twice as large after high-pressure data collection. One possible explanation for this change might be an increase in mosaic spreading of the forsterite crystal, which was signaled by the increase in diffraction diffuseness at high pressure.

Coordination polyhedral volumes and bulk moduli

Polyhedral volumes have been calculated for $M(1)$ and $M(2)$ octahedra and the silicon tetrahedron, and these volumes are given in Table 8. Distorted poly-hedra are constrained to be of smaller volume than their ideal counterparts with the same mean bond

TABLE 8. Forsterite polyhedral volumes and distortions

Site	Parameter	HCP[a]	P = 1 atm						T = 23°C			
			−196°C	23°C	~350°C[b]	~675°C[b]	~1000°C[b]	1020°C	20 kb	40 kb	50 kb	1 atm
M(1)	Octahedral Volume	$\frac{4}{3}d^3_{Mg-O}$	12.20	12.21	12.29	12.54	12.71	12.1	11.81	11.61	11.50	12.19
	Ideal Volume	$\frac{4}{3}d^3_{Mg-O}$	12.26	12.36	12.42	12.58	12.90	12.7	11.83	11.65	11.65	12.19
	Bond Angle Strain	0°	30.4	30.8	32.2	33.0	33.0	34	31.4	30.4	29.8	31.2
	Angle Variance	0°²	97.3	98.7	106.2	110.5	111.2	109	107.0	98.9	98.7	101.0
	Quadratic Elongation	1.00	1.065	1.065	1.069	1.075	1.081	1.090	1.05	1.07	1.11	1.068
M(2)	Octahedral Volume	$\frac{4}{3}d^3_{Mg-O}$	12.77	12.78	13.08	13.25	13.45	13.65	12.59	12.41	12.22	12.82
	Ideal Volume	$\frac{4}{3}d^3_{Mg-O}$	12.88	12.88	13.14	13.36	13.53	14.00	12.71	12.53	12.53	12.96
	Bond Angle Strain	0°	38.2	38.8	39.9	40.9	42.2	37.0	40.00	39.8	40.3	38.8
	Angle Variance	0°²	90.0	90.1	98.3	103.2	108.0	92	95.8	97.1	105.9	93.3
	Quadratic Elongation	1.00	1.019	1.028	1.023	1.025	1.063	1.04	1.026	1.015	1.021	1.022
Si	Tetrahedral Volume	$\frac{16}{9\sqrt{3}}d^3_{Si-O}$	2.21	2.17	2.17	2.17	2.21	2.17	2.19	2.17	2.20	2.18
	Ideal Volume	$\frac{16}{9\sqrt{3}}d^3_{Si-O}$	2.24	2.23	2.20	2.20	2.22	2.18	2.18	2.18	2.22	2.21
	Bond Angle Strain	0°	13.9	12.9	13.5	13.3	12.4	18	15.6	17.4	19	14.4
	Angle Variance	0°²	48	42	43	42	38	73	60	72	57	50
	Quadratic Elongation	1.00	1.007	1.009	1.007	1.007	1.012	1.06	1.028	1.025	1.09	1.010

a) "Ideal" hexagonal close-packed olivine model (see Fig. 1).

b) Data from Smyth and Hazen (1973).

distance; both $M(1)$ and Si are only about 1 percent smaller, whereas $M(2)$ is 2 percent smaller. While the two octahedral sites show considerable expansion and compression, the silicon tetrahedron shows no change in volume with changing T and P over the ranges studied.

Changes in polyhedral volume may be directly compared to unit-cell volume changes. From −196° to 1000°C the net change of volume in $M(1)$ and $M(2)$ is about 0.5 Å³ per octahedron, while the change in tetrahedral volume is nil. As illustrated in Figure 1, each olivine unit cell has four $M(1)$ and four $M(2)$ octahedra. Thus, cation polyhedral expansion accounts for 4.0 Å³ volume decrease per unit cell. However, the total unit-cell volume change from −196° to 1000°C is about 13 Å³, leaving 9 Å³ unaccounted for by cation polyhedral expansion. Thus, approximately 70 percent of olivine's thermal expansion may be attributed to volume increases of the unoccupied oc-

tahedral and tetrahedral sites (i.e. "voids") in the close-packed oxygen array. Magnesium octahedron expansion plays a secondary role, while tetrahedron expansion has no effect on changes in olivine's volume with temperature to 1000°C.

Similar calculations may be performed for forsterite compression. At 50 kbar, a volume decrease of approximately 0.7 Å³ in $M(1)$ and 0.5 Å³ in $M(2)$ has been recorded, thus contributing 4.8 Å³ of compression per unit cell. The total compression of magnesium olivine at 50 kbar is about 10 Å³ per unit cell. Thus, 50 percent of forsterite's compression may be ascribed to octahedral sites and 50 percent to voids, whereas silicon tetrahedra again have little effect on volume change.

Huggins (1974, p. 339 et seq.) has discussed the significance of individual polyhedral bulk moduli to the pressure response of crystalline solids. He states that systematic studies of the compressibility of poly-
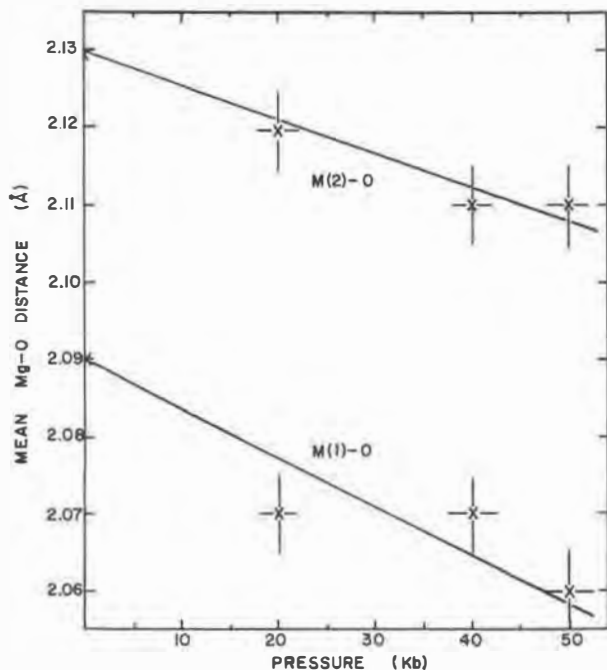
FIG. 10. Forsterite mean octahedral bond distance versus pressure.

hedra may "enable detailed predictions of crystal structures to be made at any pressure and may provide valuable insight into crystallochemical criteria for the stability of structures and into the reasons for phase changes." Bulk moduli of $M(1)$, $M(2)$, and Si are easily calculated from data in Table 8 of polyhedral volumes versus pressure by applying the equation: $K_T = -1/\beta(V) \approx -r\, dP/3\, dr$, where K_T is the bulk modulus, $\beta(V)$ is the volume compressibility, P is the pressure, and r is the interatomic distance (see e.g. Broecker and Oversby, 1971). The estimated $M(1)$ and $M(2)$ bulk moduli are thus approximately 1200 and 1000 kbar respectively at pressures between 20 and 50 kbar. These values for Mg octahedral bulk modulus are similar to the 1600 kbar bulk modulus of periclase.

The silicate tetrahedron of forsterite shows no volume compression within experimental error ($\pm$ 0.02 Å³). Therefore bulk modulus must be significantly greater than $2.2 \times 50/0.02 = 5500$ kbar. This is in agreement with Huggins (1974) estimate of $K_{Si} \approx 13,900$ kbar in andradite.

Polyhedral distortions

Characterization of polyhedral distortions is essential to an understanding of olivine crystal chemistry, and consequently, many authors have attempted to quantify these deviations from ideality. While most previous studies were designed to define the shape of olivine polyhedra (Dollase, 1974), or to plot changes in shape with changing composition (Brown, 1970; Robinson et al., 1971), these methods are equally applicable to a study of polyhedral changes with temperature and pressure. Three commonly cited distortion indices have been calculated and are tabulated in Table 8. These are: (1) bond angle strain, (2) polyhedral angle variance, and (3) mean polyhedral elongation. Each is a measure of the deviation from a regular polyhedral form, and each has been applied with good results to the olivine group.

Several generalizations may be made regarding the effects of temperature and pressure on forsterite polyhedral distortions, as measured by the three distortion indices. The two magnesian olivine octahedral sites display very similar behavior. Both exhibit strong increasing distortions with increasing temperature, but little, if any, change with increasing pressure. This pattern may be explained in terms of the trends of expansion and compression of individual Mg–O bonds, as shown in Figure 6. Since longer bonds will expand up to four times more rapidly than shorter bonds, an increase in temperature will result in increased variance of bond distances, and corresponding increases in distortion. Conversely, an increase in pressure will force a decrease in the range of bond distances, and perhaps a reduction in octahedral distortions. The fact that a definite trend towards reduction in octahedral distortions was not observed at high pressures may be due in part to nonhydrostatic conditions at high pressure. Further high-pressure structure refinements are needed to clarify octahedral distortion behavior.

Tetrahedral distortions are small compared to those of the two octahedral sites. Virtually no changes in distortions occur between −196° and 1000°C, though some fluctuations (within experimental error) are observed. However, a general increase of tetrahedral distortions is seen with increasing pressure. Whether this increase is due to nonhydrostatic effects, or to real distortion, is not clear. However, it should again be emphasized that errors in forsterite bond angles and bond distances are large, and that all distortion calculations are based on *differences* between these numbers of similar size. Therefore, additional data are required to resolve the nature of silicon tetrahedral distortions with pressure.

Conclusions

Development within the past decade of high-temperature, low-temperature, and high-pressure diffrac-

tion apparatus now permits the study of mineral crystal structures over a range of pressure and temperature. This investigation concentrated on the complex pressure and temperature response of the magnesian olivine forsterite. Significant differences were observed in the thermal expansion and compressibility of magnesium octahedra versus silicon tetrahedra, reflecting the differences in charge and coordination of these two cations. Furthermore, within each polyhedron a range of individual bond expansions was noted, with longer bonds expanding more rapidly than shorter bonds. These data will be combined in a subsequent study with data on iron-bearing olivines in an effort to predict the structure and stability, as a function of composition, temperature, and pressure for the ferromagnesian olivines.

Acknowledgments

References

Belov, N. V., E. N. Belov, N. N. Andrianova and R. F. Smirnova (1951) Determination of the parameters in the olivine (forsterite) structure with the harmonic 3-D synthesis. *C. R. Acad. Sci. USSR,* **81,** 399–402.

Birle, J. D., G. V. Gibbs, P. B. Moore and J. V. Smith (1968) Crystal structures of natural olivines. *Am. Mineral.* **53,** 807–824.

Bragg, W. L. and G. B. Brown (1926) Die Struktur des Olivines. *Z. Kristallogr.* **63,** 538.

Bridgman, P. W. (1948) Rough compression of 177 substances to 40,000 kg/cm². *Proc. Am. Acad. Arts Sci.* **76,** 71–87.

Broecker, W. S. and V. M. Oversby (1971) *Chemical equilibria in the Earth.* McGraw-Hill, New York, 318 p.

Brown, G. E. (1970) *Crystal Chemistry of the Olivines.* Ph. D. Thesis, Virginia Polytechnic Institute, Blacksburg, Virginia.

—— and C. T. Prewitt (1973) High–temperature crystal chemistry of hortonolite. *Am. Mineral* **58,** 577–587.

Burnham, C. W. (1965) Temperature parameters of silicate crystal structures (abstr). *Am. Mineral.* **50,** 282.

Busing, W. R. and H. A. Levy (1964) The effect of thermal motion on the estimation of bond lengths from diffraction measurements. *Acta Crystallogr.* **17,** 142–146.

Dollase, W. A. (1974) A method of determining the distortion of coordination polyhedra. *Acta Crystallogr.* **A30,** 513–517.

Finger, L. W. (1969) Determination of cation distribution by least-squares refinement of single-crystal X-ray data. *Carnegie Inst. Wash. Year Book,* **67,** 216–217.

Hanke, K and J. Zemann (1963) Verfeinerung der Kristallstruktur von Olivin. *Naturwissenschaften* **50,** 91–92.

Hazen, R. M. (1976) Effects of temperature and pressure on the cell dimension and X-ray temperature factors of periclase. *Am. Mineral.* **61,** 266–271.

—— and C. W. Burnham (1974) The crystal structures of gillespite I and II: a structure determination at high pressure. *Am. Mineral.* **59,** 1166–1176.

——, and —— (1975) The crystal structure of gillespite II at 26 kilobars: Correction and addenda. *Am. Mineral.* **60,** 937–938.

Heinriques, Â. (1957) The effect of cations on the optical properties and cell dimensions of knebelite and olivine. *Arkiv Mineral. Geol.* **2,** 305–313.

Huggins, F. (1974) *Mössbauer studies of iron minerals under pressures of up to 200 kilobars.* Ph. D. Thesis, Massachusetts Institute of Technology, Cambridge, Massachusetts.

Kozu, S., J. Ueda and S. Tsurumi (1934) Thermal expansion of olivine. *Imp. Acad. Japan Proc.* **10,** 83–86.

Louisnathan, S. J. and J. V. Smith (1968) Cell dimensions of olivine. *Mineral. Mag.* **36,** 1123–1134.

Olinger, B. and A. Duba (1971) Compression of olivine to 100 kilobars. *J. Geophys. Res.* **76,** 2610–2616.

—— and P. M. Halleck (1975) Redetermination of the relative compression of the cell edges of olivine. *J. Geophys. Res.* **80,** (in press)

Rigby, G. R., G. H. B. Lovell and A. T. Green (1946) The reversible thermal expansion and other properties of some magnesian ferrous silicates. *Trans. Brit. Ceram. Soc.* **45,** 237–250.

Robinson, K., G. V. Gibbs and P. H. Ribbe (1971) Quadratic elongation: a quantitative measure of distortion in coordination polyhedra. *Science,* **172,** 567–570.

Schock, R. N., B. Olinger and A. Duba (1972) Additional data on the compression of olivine to 140 kilobars. *J. Geophys. Res.* **77,** 382–384.

Skinner, B. J. (1962) Thermal expansion of ten minerals. *U. S. Geol. Surv. Prof. Pap.* **450D,** 109–112.

Smyth, J. R. (1973) An orthopyroxene structure up to 850°C. *Am. Mineral.* **58,** 636–648.

——(1975) High temperature crystal chemistry of fayalite. *Am. Mineral.* **60,** 1092–1097.

——and R. M. Hazen (1973) The crystal structures of forsterite and hortonolite at several temperatures up to 900°. *Am. Mineral.* **58,** 588–593.

Soga, N. and O. L. Anderson (1967) High-temperature elasticity and expansivity of forsterite and steatite. *J. Am. Ceram. Soc.* **50,** 239–242.

Yoder, H. S. and T. G. Sahama (1957) Olivine X-ray determinative curve. *Am. Mineral.* **42,** 475–491.